<14) hydrogen bonding to the oxydianion in the wild-type SBP (*8*).

Although the active site Ser in proteinases has been successfully mutated to Cys, the ultimate goal or desired result has not been achieved; engineered thiol trypsin exhibits essentially no enzymatic activity with normal amide and ester substrates (*3*). The cause of the failure to achieve the desired result is not clearly understood (*15*). Small geometrical changes resulting from the mutation could have an effect far more profound than that described here. Although little publicized, the catalytic Ser or Cys residues of proteolytic enzymes are, like Ser^{130} of SBP, engaged in cooperative hydrogen bonding; they simultaneously donate to a His residue that is part of the charge relay system and accept an NH group or a solvent molecule.

The results presented here demonstrate the sensitivity of a Ser to Cys mutation. If the effect of the mutation is as deleterious as the one reported here, one wonders what the extent of the effect might be if the residue is directly involved in enzyme catalysis. In any case the use of site-directed mutagenesis to probe or quantitate structure-function relations is fraught with uncertainty. To minimize the uncertainty, it is important that many mutational changes be made. For amino acid replacements to be rationally selected and generated and for interpretation of the results to be properly made, a well-refined high-resolution structure is a prerequisite.

Finally, there seems to be a propensity of hydroxyl-containing residues, as well as peptide units, to interact with charged groups and ligands (*9, 16, 17*). An excellent example has been recently shown in the well-refined 1.7 Å resolution structure of the phosphate-binding protein in complex with phosphate; the completely dehydrated and sequestered phosphate is held in place by a total of 12 hydrogen bonds, 5 with peptide unit NH groups and 4 with hydroxyl side chains (*17*). We have further noted that ligand-gated ion channels are known to contain regions rich in hydroxyl side chains and that, like in the binding protein-phosphate complex, these hydroxyls may have properties that are particularly important in achieving the requisite specificity and speed of ion movements (*17*). The sensitivity and differential effects of mutations of Ser to Cys, Ala, and Gly at a highly specific ion-binding site as demonstrated here could be used to probe similar residues residing in these channels or in other ligand-binding sites.

REFERENCES AND NOTES

1. L. Polger and M. L. Bender, *J. Am. Chem. Soc.* **88**, 153 (1966).
2. K. E. Neet and D. E. Koshland, *Proc. Natl. Acad. Sci. U.S.A.* **56**, 1606 (1966).
3. J. N. Higaki *et al.*, *Biochemistry* **28**, 9256 (1989).
4. C. E. Furlong, in *Cellular and Molecular Biology*, F. C. Neidhardt, Ed. (American Society for Microbiology, Washington, DC, 1987), pp. 768–796; G.F.-L. Ames, *Annu. Rev. Biochem.* **55**, 397 (1986); F. A. Quiocho, *Philos. Trans. R. Soc. London Ser. B* **326**, 341 (1990).
5. H. Isihara and R. W. Hogg, *J. Biol. Chem.* **255**, 4614 (1980).
6. B. L. Jacobson *et al.*, *ibid.*, in press.
7. A. B. Pardee, *ibid.* **241**, 5886 (1966).
8. B. L. Jacobson and F. A. Quiocho, *J. Mol. Biol.* **204**, 783 (1988).
9. J. W. Pflugrath and F. A. Quiocho, *Nature* **314**, 257 (1985); *J. Mol. Biol.* **200**, 163 (1988).
10. J. S. Sack and F. A. Quiocho, in preparation.
11. The expression vectors and methods used in the mutagenesis in *E. coli* have been described (*6*). Mutations of $Ser^{130} \rightarrow$ Gly, $Ser^{130} \rightarrow$ Ala, and $Ser^{130} \rightarrow$ Cys and were directed by oligonucleotides 5′-CGCCACCACCGCTTTTC-3′, 5′-CGCCACCAGCGCTTTTC-3′, and 5′-CGCCACCACAGCTTTTC-3′, respectively, where the bold underlined base indicates mismatches. In each mutagenesis, the entire SBP gene was sequenced to ensure that the desired mutation was attained.
12. Proteins were purified from a 12-liter growth of appropriate mutant *E. coli* cells with the use of the method previously described for the wild-type SBP (*5, 6*). Purification of SBP with this method is achieved mainly by the use of DEAE-53 ion exchange chromatography. The Ala^{130} and Gly^{130} SBP mutants were further purified by high-performance liquid chromatography (HPLC) with a preparative Synchrom Q300 anion exchange column. In the purification of the Ser^{130}Cys mutant, β-mercaptoethanol was added to all solutions to a final concentration of 1 mM. Moreover, after chromatography on a DEAE column, the mutant protein was further purified by isoelectric focusing (ampholyte pH 6 to 8) with a Bio-Rad Rotofor Preparative IEF Cell. Protein purity was determined by SDS-polyacrylamide gel electrophoresis and isoelectric focusing with Pharmacia's PhastGel. Protein concentration was determined spectrophotometrically by using an extinction coefficient of 1.2 ml mg^{-1} cm^{-1} (*7*).
13. Note that the binding activity of Gly^{130} and Ala^{130} SBP mutants was measured at pH 7.5, the pH at which the wild-type protein activity is normally measured (*7, 8*). The Cys^{130} SBP mutant has maximum activity at about pH 6.0 (see Table 1).
14. M. M. Frey *et al.*, *Acta Crystallogr.* **B29**, 876 (1973); T. J. Kistenmacher *et al.*, *ibid.* **B30**, 2573 (1974); A. K. Kerr *et al.*, *ibid.* **B31**, 2022 (1975).
15. M. E. McGrath *et al.*, *Biochemistry* **28**, 9264 (1989).
16. F. A. Quiocho *et al.*, *Nature* **329**, 561 (1987).
17. H. Luecke and F. A. Quiocho, *ibid.* **347**, 402 (1990).

18. We thank B. L. Jacobson, J. C. Spurlino, and P. S. Vermersch for their assistance and helpful discussions. Supported in part by grants from NIH and the Welch Foundation.

10 October 1990; accepted 27 December 1990

Crystal Structure of Defensin HNP-3, an Amphiphilic Dimer: Mechanisms of Membrane Permeabilization

CHRISTOPHER P. HILL, JEFF YEE,* MICHAEL E. SELSTED,† DAVID EISENBERG

Defensins (molecular weight 3500 to 4000) act in the mammalian immune response by permeabilizing the plasma membranes of a broad spectrum of target organisms, including bacteria, fungi, and enveloped viruses. The high-resolution crystal structure of defensin HNP-3 (1.9 angstrom resolution, *R* factor 0.19) reveals a dimeric β sheet that has an architecture very different from other lytic peptides. The dimeric assembly suggests mechanisms by which defensins might bind to and permeabilize the lipid bilayer.

NEUTROPHILS CONSTITUTE 50 TO 70% of the total white blood cells in humans. They play a vital role in the immune response by ingesting invading microorganisms, which are then destroyed by one of two general mechanisms. The "oxygen-dependent" mechanism results from the production of superoxide, which is converted to potent oxidants termed "reactive oxygen intermediates" (*1*). The other, "oxygen-independent," defense mechanism occurs when the microbicidal-cytotoxic proteins of cytoplasmic granules are discharged into the phagocytic vacuole (*2*).

Defensins account for ~30% of the total protein in human azurophil granules (*3*). They are small (molecular weight of 3500 to 4000), cationic, disulfide cross-linked proteins that show in vitro activity against Gram-negative and Gram-positive bacteria (*3, 4*), fungi (*5*), mammalian cells (*6*), and enveloped viruses (*7*). The work of Lehrer and colleagues shows that defensins permeabilize both the inner and outer membranes of *Escherichia coli*, and that inner-membrane permeabilization is coincident with cell death (*8*). A membrane potential is apparently required for defensin action, since cells are killed only when metabolically active and they are protected by membrane-depolarizing agents such as carbonylcyanide M-chlo-

C. P. Hill, J. Yee, D. Eisenberg, Molecular Biology Institute and Departments of Chemistry and Biochemistry, University of California, Los Angeles, CA 90024–1570.
M. E. Selsted, Departments of Medicine and Pathology, University of California, Los Angeles, CA 90024–1732.

*Present address: University of California College of Medicine, Irvine, CA 92717.
†Present address: Department of Pathology, University of California College of Medicine, Irvine, CA 92717.

rophenylhydrazone (CCCP) and 2,4-dinitrophenol (DNP) (*8, 9*). This result is consistent with the observation that defensins form voltage-dependent channels in lipid bilayers, a process that apparently involves aggregation of two to four molecules (*10*). These data strongly suggest that defensins kill by permeabilizing the membrane; so does their broad specificity, which includes enveloped but not naked viruses (*7*).

To understand further the mechanism of defensin action we have determined the crystal structure of the defensin HNP-3 by the method of isomorphous replacement (Table 1) and refined the atomic model to an *R* factor of 0.19 against 1.9 Å data (Table 2). The structure we see is remarkable in being quite unlike that of other membrane-permeabilizing proteins. Other lytic or membrane-permeabilizing peptides have been characterized, including melittin (*11*), cecropin (*12*), magainin (*13*), alamethicin (*14*), and δ-hemolysin (*15*). All of these are amphiphilic α helices that contain no β sheet and have no disulfide bonds. In sharp contrast, defensin is an all–β-sheet protein with no α helix, and it is stabilized by three disulfide bonds. The few membrane-permeabilizing proteins that do contain significant amounts of β sheet are either circular peptides, such as gramicidin S (*16*), or contain D-amino acids, such as gramicidin A (*17, 18*), or, like porin (*19*), are much larger than defensin.

Defensin is an elongated, ellipsoidal molecule with overall dimensions of 26 Å by 15 Å by 15 Å (Fig. 1A). The structure is

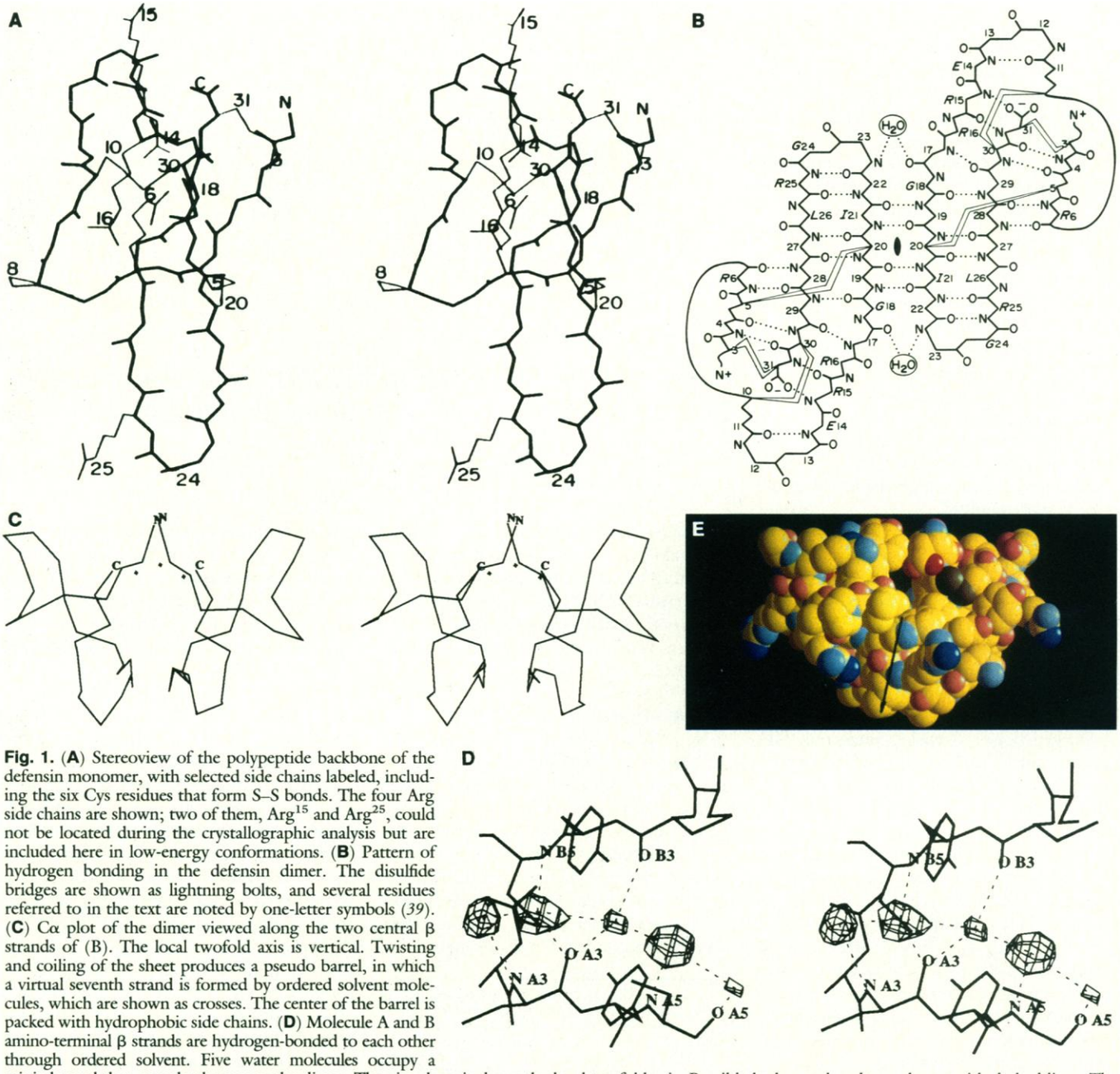

Fig. 1. (**A**) Stereoview of the polypeptide backbone of the defensin monomer, with selected side chains labeled, including the six Cys residues that form S–S bonds. The four Arg side chains are shown; two of them, Arg^{15} and Arg^{25}, could not be located during the crystallographic analysis but are included here in low-energy conformations. (**B**) Pattern of hydrogen bonding in the defensin dimer. The disulfide bridges are shown as lightning bolts, and several residues referred to in the text are noted by one-letter symbols (*39*). (**C**) Cα plot of the dimer viewed along the two central β strands of (B). The local twofold axis is vertical. Twisting and coiling of the sheet produces a pseudo barrel, in which a virtual seventh strand is formed by ordered solvent molecules, which are shown as crosses. The center of the barrel is packed with hydrophobic side chains. (**D**) Molecule A and B amino-terminal β strands are hydrogen-bonded to each other through ordered solvent. Five water molecules occupy a mini-channel that completely crosses the dimer. The view here is down the local twofold axis. Possible hydrogen bonds are shown with dashed lines. The $F_{obs} - F_{calc}$ map was computed with all water molecules deleted from the model; it was contoured at 3.5 times the root-mean-square deviation. (**E**) Space-filling representation of the dimer with the local twofold axis vertical and viewed along the solvent mini-channel, which can be seen at the top center. Carbon atoms, yellow; sulfur, brown; uncharged nitrogen, light blue; charged nitrogen, blue; uncharged oxygen, pink; and charged oxygen, red. Notice that the base of the basket is apolar, as shown by the hydrophobic moment (black arrow), which points toward the base.

dominated by a three-stranded antiparallel β sheet that includes 60% of all residues (*20–24*). The molecule appears sufficiently rigid that the crystal structure must provide a good model both for the conformation in solution and at the site of action. The constraints of the three disulfide bonds prohibit a gross conformational change, such as that proposed for colicin A (*25*), upon moving from an aqueous to an apolar milieu. This appearance of stability is supported by the similarity of the two molecules in the asymmetric unit. All main-chain atoms of the two molecules superpose with a root-mean-square (rms) deviation of 0.82 Å. The only significant departure from noncrystallographic symmetry is an apparent flexing motion of residues 20 to 25. If these residues are omitted from the least squares superposition, the deviation of main-chain atoms of the two monomers becomes 0.32 Å.

The pattern of conserved residues of the defensin family (Fig. 2) can be interpreted in terms of the three-dimensional structure and suggests that all other defensins have conformations similar to HNP-3. The six Cys residues that must play a major role in stabilizing the conformation are invariant. Moreover, several other key structural residues, Arg^6, Glu^{14}, and Gly^{24}, are found in every defensin except GPNP. Gly^{24} occupies the third position of a type I′ turn; Arg^6 forms a salt bridge with Glu^{14} that spans the only stretch of polypeptide that does not participate in the β sheet (*26*). Nuclear magnetic resonance (NMR) studies of NP-5 (*27–29*) also support the view that all known defensin sequences can fold as HNP-3.

HNP-3 crystallizes as a dimer. The two molecules in the asymmetric unit are in close contact and are related to each other by a local twofold rotation axis. The three-stranded β sheet of the monomer is extended across this interface to form a six-stranded sheet in the dimer. Figure 1B shows how four hydrogen bonds link the two monomer sheets directly and that two more hydrogen bonds extend the intermolecular β-sheet interaction through well-ordered water molecules. The dimeric association is further stabilized by hydrophobic interactions, especially between Cys^5, Cys^{20}, Tyr^{22}, and Phe^{28} from each of the monomers. Equilibrium centrifugation confirmed that HNP-3 is a dimer or higher polymer in solution under conditions identical to the crystallization conditions but without the PEG 8000 (*30*). The presence of the invariant Gly^{18} at the dimer interface also suggests that defensin is a dimer at the site of action. If Gly^{18} were replaced by any other residue, the Cβ atom would overlap with the O atom of residue 20 from the neighboring monomer. The observed dimeric association suggests several hypotheses for the killing mechanism of defensins, as discussed below.

The shape of the dimer resembles a basket with an apolar base and a polar top that includes the two amino termini and the two carboxyl termini (Figs. 1C and 3A). The β sheet both twists and coils, and as a result the amino-terminal β strands of the two neighboring monomers are close together in space (Fig. 1C). These two β strands are hydrogen-bonded together through ordered solvent molecules that form a mini-channel, which passes right through the dimer (Fig. 1, D and E). The core of this basket is hydrophobic and, at the center of the dimer interface, the disulfide bonds between residues 5 and 20 of the two molecules are in van der Waals contact with each other. Six Arg residues form an equatorial ring around the dimer; these side chains are relatively flexible and three of them cannot be located in Fourier maps.

The dimeric crystal structure suggests

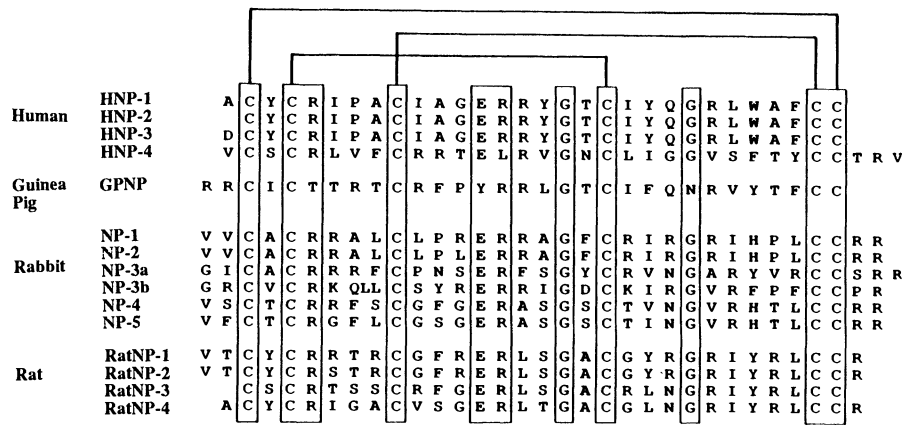

Fig. 2. The amino acid sequences of HNP-3 and other defensins (*39, 40*) are referred to a common numbering scheme. As a result the 30-residue HNP-3 starts with residue number 2 and ends with residue number 31. The disulfide connectivity is indicated and residues are boxed if conserved in at least all but one of the sequences.

Table 1. Data collection and structure determination. HNP-3 was purified as described (*34*), and crystals were grown at room temperature in 4-μl hanging drops. The drop consisted of a 50:50 mixture of reservoir and 20 mg ml^{-1} protein in 0.01% acetic acid, the reservoir solution was 15% PEG 8000, 10% isopropanol, 100 mM sodium citrate at pH 4.0. Crystals would usually grow in about 4 days and were harvested into the reservoir solution without loss of diffraction properties. The space group is $P2_12_12$ with a = 30.8 Å, b = 45.0 Å, and c = 40.3 Å. There are two defensin monomers in the asymmetric unit, and the crystal contains 38% solvent. These HNP-3 crystals are apparently isomorphous to one of the forms reported for the closely related HNP-1 (*35*). A total of six derivatives were identified by locating the heavy-atom positions by using Patterson and Fourier methods. Inspection of several Fourier maps showed density that clearly corresponded to a Trp side chain. Once this feature had been recognized, many maps calculated with the use of different combinations of derivatives, with and without solvent flattening (*36*), were assayed by the quality of this Trp density. The best map was that calculated from $K_2Pt(CN)_4$ (20 mM, 24-hour soak, three sites) and $Pt(NH_2)_2(NO_2)_2Cl_2$ derivatives (13 mM, 4.5-day soak, one site) after solvent flattening. Maps phased on both of these derivatives but before solvent leveling, or based on just the $K_2Pt(CN)_4$ derivative after solvent flattening, were also of high quality. The mean figure of merit after solvent flattening was 0.73. These three maps were displayed on an Evans and Sutherland PS390, and an atomic model was easily fitted with the program FRODO (*37*).

Parameter	Native	$K_2Pt(CN)_4$	$Pt(NH_2)_2$-$(NO_2)_2Cl_2$
R_{iso}*		0.16	0.11
Resolution limit (d_{min}, Å)	1.9	2.4	2.5
Observations (no.)	22,975	18,559	16,019
Rejected during processing (no.)	1,617	179	850
Unique reflections (no.)	4,524	2,390	2,128
% Complete	(95.9)	(99.5)	(99.4)
$\|F\| > 2\sigma_F$ (%)	96.7	97.7	98.9
R_{sym}†	0.054	0.048	0.057
Rms F_h/E‡ (centrics)		1.38	0.70
Rms F_h/E (acentrics)		1.57	0.94
R_{Cullis}§		0.53	0.70

*$R_{iso} = (\sum | F_{derivative} | - | F_{native} |)/\sum | F_{native} |$. †$R_{sym} = (\sum | I_i | - | I_{av} |)/\sum | I_{av} |$; this value is calculated before rejecting any observations. ‡F_h is the heavy-atom structure factor and E is the residual lack of closure. §$R_{Cullis} = (\sum | F_{h(obs)} | - | F_{h(calc)} |)/\sum | F_{h(obs)} |$.

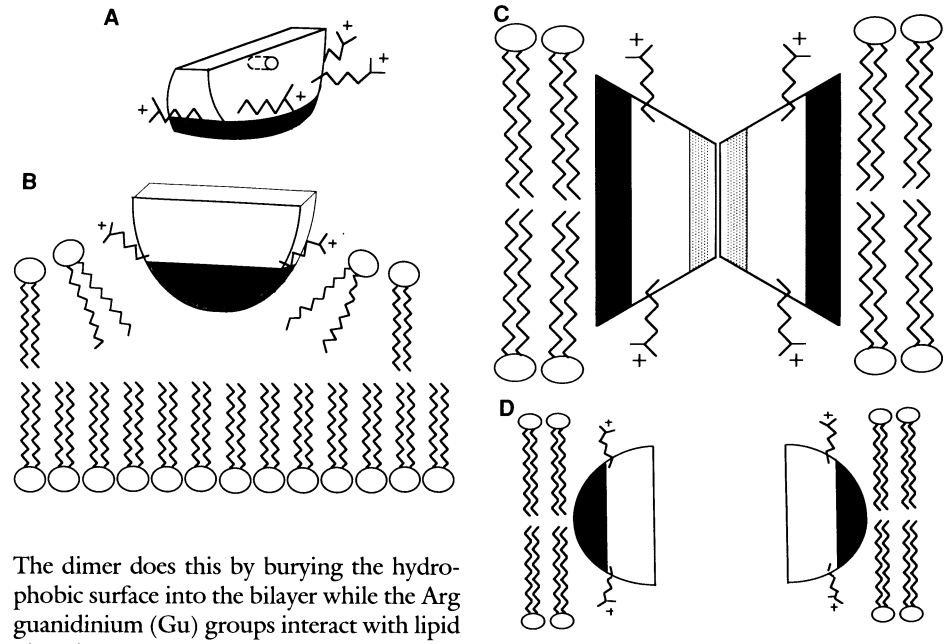

Fig. 3. (**A**) Schematic representation of the dimer basket. The top is hydrophilic, and the base is hydrophobic (shaded). Six flexible Arg residues are distributed around the middle. The solvent mini-channel is indicated. The local twofold is vertical. (**B**) Wedge hypothesis. The hydrophobic surface of the dimer is buried into the lipid bilayer, disrupting the lipid-lipid interactions and perhaps permeabilizing the membrane. (**C**)) Dimer-pore hypothesis. Two dimers stack top to top with their bottom hydrophobic surfaces (shaded) facing lipid tails. Association of the hydrophilic top surfaces is stabilized by charge complementarity. Two solvent mini-channels (stipled) cross the bilayer. (**D**) General-pore hypothesis. This cross section shows just two defensin dimers. In order to complete the pore, more dimers must be added in front and back. Modeling suggests that at least four dimers are required to complete this type of pore, which could include many defensin molecules and become very large.

three ways in which defensin molecules might interact with and permeabilize a lipid bilayer. A wedge effect, like that proposed for the permeabilization of membranes by melittin and lysolecithin (*31*), might result from the amphiphilicity of the dimer basket. A cluster of four hydrophobic side chains on the bottom of the basket (Figs. 1C and 3A) provides a hydrophobic patch of 344 Å^2 of solvent-accessible surface area that is surrounded, further up the basket, by the ring of six Arg side chains. In the wedge hypothesis, the HNP-3 dimer disrupts the membrane by distorting lipid-lipid interactions. The dimer does this by burying the hydrophobic surface into the bilayer while the Arg guanidinium (Gu) groups interact with lipid phosphate groups (Fig. 3B).

Two other possible mechanisms emerge from the structure, both of which involve pore formation. One of these, the dimer pore, makes use of the solvent mini-channel seen in the crystal structure (Fig. 1, D and E). In this model, two dimers assemble in the membrane with their polar tops toward each other and apolar bases facing lipid tails (Fig. 3C). There is some charge complementarity at this putative dimer-dimer interface, especially involving the ion pair Arg^6 and Glu^{14}. The side chains of the six "equatorial" Arg residues move to bind lipid head groups. In this configuration, two of the solvent mini-channels seen in the crystal structure completely span the bilayer.

The other, general-pore, hypothesis also has dimers completely spanning the membrane, but now rotated by ~90° from the "dimer-pore" orientation and with the polar top surface lining the pore (Fig. 3D). The same hydrophobic dimer surface contacts lipid tails, and Arg side chains have again moved to bind head groups. Simple modeling suggests that at least four dimers are required to form this type of pore, which could conceivably become very large and include many defensin dimers.

At this stage it is not possible to tell which, if any, of these three ideas are correct. Indeed they might all have elements of correctness, since a wedge interaction could be the forerunner of either of the other two "pore" models. The concentration dependence of defensin activity (*10*) might reflect transitions from wedge to dimer-pore to general-pore mechanisms.

Each of the three models requires burying essentially the same hydrophobic surface against the lipid aliphatic chains, binding of the same Arg Gu functions to lipid head groups, and exposing the same hydrophilic surface to a suitable environment. Consequently, consideration of the various defensin sequences may support each model, but will not in general allow us to choose among them. The greatest challenge to the three hypotheses is the presence of Asp^{18} in NP-3b, which in all the models is buried in the middle of the membrane. Consideration of Arg^{16} suggests that this is not a fatal flaw in

Table 2. Refinement statistics for the atomic model in which the restrained least squares program of Hendrickson was used (*38*).

Refinement parameter	Value
Resolution range (Å)	1.9–10.0
Reflections (no.)	4448
R factor*	0.190
Protein atoms included (no.)	270
Protein atoms missing (no.)	12
Water molecules included (no.)	44
B factor: Wilson plot (2.5–1.9 Å) (Å^2)	15.6
B factor: Molecule A average (Å^2)	14.5
B factor: Molecule B average (Å^2)	17.9
B factor: Solvent average (Å^2)	38.3
(1–2) Bond distances (Å)†	0.019 (0.020)
(1–3) Angle distances (Å)	0.049 (0.040)
(1–4) Distances (Å)	0.045 (0.050)
Planarity (Å)	0.014 (0.020)
Chiral volumes (Å^3)	0.180 (0.150)
Nonbonded contacts (Å)	
Single torsion	0.204 (0.500)
Multiple torsion	0.274 (0.500)
Possible hydrogen bonds	0.181 (0.500)
Conformation torsion angles (degrees)	
Planar (0°, 180°)	2.8 (3.0)
Staggered (±60°, 180°)	18.2 (15.0)
Orthonormal (±90°)	28.8 (20.0)
Isotropic temperature factors (Å^2)	
Main-chain bond	0.991 (1.000)
Main-chain angle	1.720 (1.500)
Side-chain bond	1.565 (1.000)
Side-chain angle	2.427 (1.500)

*$R = (\Sigma \mid F_{obs} \mid - \mid F_{calc} \mid)/\Sigma \mid F_{obs} \mid$. †The values are the rms deviations; the target σ values are given in parentheses.

our models; Arg^{16} is conserved betwen HNP-3 and NP-3b, and in the HNP-3 crystal structure this Gu forms a hydrogen bond with Thr^{18} (equivalent to Asp^{18} of NP-3b). In each of our three hypothetical membrane-bound models the Arg^{16} side chain can be repositioned so that its methylene groups contact lipid tails while its Gu group binds lipid head groups. Perhaps in NP-3b the Arg^{16} Gu maintains a salt bridge with Asp^{18} within the hydrophobic lipid environment. Such intramembrane salt bridges have precedence (*32*). Despite the high degree of defensin sequence variation, the flexibility of Arg side chains and plasticity of the membrane suggests that the different defensins could all interact with membranes in an identical manner.

All three of the hypotheses are consistent with the observation that a membrane potential is required for defensin activity (*8, 9*). In the wedge model the net negative charge on the inside of the cell drives the cationic wedge into the bilayer. In the pore models the potential is required to pull some of the Arg side chains completely across the membrane. All three models also rationalize the observed biphasic binding kinetics (*5*), in which the first step is predominantly electrostatic (Arg side chains with head groups) and the second of a more hydrophobic nature with lipid functions that are initially cryptic (hydrophobic dimer surface with lipid tails).

Defensin shares more in structural characteristics with small toxins that act by binding to specific receptor proteins than with other lytic peptides. Defensin's overall dimensions, positive charge, β sheet, and disulfide bonds are reminiscent of various snake, scorpion, and spider toxins (*33*) that function not by permeabilizing the membrane, but by binding molecules such as the acetylcholine receptor. Although similar to these, the defensin structure is quite different from other membrane-permabilizing peptides. The constrained, disulfide cross-linked structure, common to defensins and the small toxins, may reflect a requirement to maintain a stable and compact conformation to avoid digestion by proteases.

REFERENCES AND NOTES

1. C. J. White and J. I. Gallin, *Clin. Immunol. Immunopathol.* **40**, 50 (1986); S. J. Klebanoff, in *Inflammation: Basic Principles and Clinical Correlates*, J. I. Gallin, I. M. Goldstein, R. Snyderman, Eds. (Raven, New York, 1988), pp. 391–444.
2. R. I. Lehrer, T. Ganz, M. E. Selsted, *Hematol. Oncol. Clin. North Am.* **2**, 159 (1988).
3. G. I. Greenwald and T. Ganz, *Infect. Immun.* **55**, 1365 (1987).
4. M. E. Selsted *et al.*, *ibid.* **45**, 150 (1984).
5. R. I. Lehrer *et al.*, ibid. **49**, 207 (1985).
6. A. Lichtenstein *et al.*, *Blood* **68**, 1407 (1986).
7. R. I. Lehrer *et al.*, *J. Virol.* **54**, 467 (1985); K. A. Daher *et al.*, *ibid.* **60**, 1068 (1986).
8. R. I. Lehrer *et al.*, *J. Clin. Invest.* **84**, 553 (1989).
9. R. I. Lehrer *et al.*, *Blood* **72**, 149a (1988).
10. B. L. Kagan, M. E. Selsted, T. Ganz, R. I. Lehrer, *Proc. Natl. Acad. Sci. U.S.A.* **87**, 210 (1990).
11. T. C. Terwilliger and D. Eisenberg, *J. Biol. Chem.* **257**, 6010 (1982).
12. T. A. Holak *et al.*, *Biochemistry* **27**, 7620 (1988).
13. M. Zasloff, *Proc. Natl. Acad. Sci. U.S.A.* **84**, 5449 (1987).
14. R. O. Fox and F. M. Richards, *Nature* **300**, 325 (1982).
15. K. H. Lee, J. E. Fitton, K. Wuthrich, *Biochim. Biophys. Acta* **911**, 144 (1987).
16. S. E. Hull, R. Karlsson, P. Main, M. M. Woolfson, E. J. Dodson, *Nature* **275**, 206 (1978).
17. B. A. Wallace and K. Ravikumar, *Science* **241**, 182 (1988).
18. D. A. Langs, *ibid.*, p. 188.
19. C. Paul and J. P. Rosenbusch, *EMBO J.* **4**, 1593 (1985); B. K. Jap, *J. Mol. Biol.* **205**, 407 (1989); M. S. Weiss *et al.*, *FEBS Lett.* **256**, 143 (1989).
20. Secondary structure was defined with the program DSSP (*21*). The first β strand, residues 4 to 6, is followed by a type VI turn (*22*) formed by residues 6 to 9, the third residue of which, Pro^8, is preceded by a cis peptide bond. Residues 9 to 11 are extended but without backbone hydrogen bonds. Then residues 11 to 14 form a type II turn with a hydrogen bond between 11 O and 14 N. At residue 15, the chain continues with a long β strand and then forms a type I′ hairpin at residues 22 to 25. The final β strand consists of residues from Gly^{24} through the carboxyl terminus. The β sheet is twisted in the usual sense (*23*), and this twist is exaggerated by a β bulge (*24*) formed by residues 17, 18, and 29.
21. W. Kabsch and C. Sander, *Biopolymers* **22**, 2577 (1983).
22. P. N. Lewis, F. A. Momany, H. A. Scheraga, *Biochim. Biophys. Acta* **303**, 211 (1973).
23. C. Chothia, *J. Mol. Biol.* **75**, 295 (1973).
24. J. S. Richardson, E. D. Getzoff, D. C. Richardson, *Proc. Natl. Acad. Sci. U.S.A.* **75**, 2574 (1978).
25. M. W. Parker *et al.*, *Nature* **337**, 93 (1989).
26. The GPNP sequence does not seem to be an exception: the Thr and Tyr that replace Arg^6 and Glu^{14} in GPNP do not seem to disrupt the structure, but rather fill the same volume as the Arg and Glu side chains in HNP-3; also a hydrogen bond can probably be formed between GPNP Thr^6 $O\gamma^1$ and Tyr^{14} $O\eta$.
27. NMR studies on NP-5 (*28, 29*), which show a β hairpin formed by residues 19 to 28 and a type I′ turn formed by residues 22 to 25, in general agreement with the HNP-3 crystal structure. The crystal structure of HNP-3 differs, however, from the NMR structure in details. For example, the crystal structure includes a third β strand formed by residues 4 to 6. This strand has not been described for NP-5, although inspection of stereo figures in (*29*) indicates that the NMR conformation in this region is similar to that in HNP-3 crystals.
28. A. C. Bach, M. E. Selsted, A. Pardi, *Biochemistry* **26**, 4389 (1987).
29. A. Pardi *et al.*, *J. Mol. Biol.* **201**, 625 (1988).
30. P. Poon and V. Schumaker, personal communication.
31. D. A. Haydon and J. Taylor, *J. Theor. Biol.* **4**, 281 (1963); C. R. Dawson *et al.*, *Biochim. Biophys. Acta* **510**, 75 (1978); J. G. Mandersloot *et al.*, *ibid.* **382**, 22 (1975).
32. K. Oosawa and M. Simon, *Proc. Natl. Acad. Sci. U.S.A.* **83**, 6930 (1986).
33. W. Massefski, Jr. *et al.*, *Science* **249**, 521 (1990); M. D. Walkinshaw *et al.*, *Proc. Natl. Acad. Sci. U.S.A.* **77**, 2400 (1980); B. Rees *et al.*, *J. Mol. Biol.* **214**, 281 (1990); J. C. Fontecilla-Camps *et al.*, *Proc. Natl. Acad. Sci. U.S.A.* **85**, 7443 (1988); J. C. Fontecilla-Camps *et al.*, *Trends Biochem. Sci.* **6**, 291 (1981).
34. T. Ganz *et al.*, *J. Clin. Invest.* **76**, 1427 (1985).
35. R. L. Stanfield, E. M. Westbrook, M. E. Selsted, *J. Biol. Chem.* **263**, 5933 (1988).
36. B.-C. Wang, *Methods Enzymol.* **115**, 90 (1985).
37. T. A. Jones, *ibid.*, p. 157.
38. W. A. Hendrickson, *ibid.*, p. 252.
39. Abbreviations for the amino acid residues are A, Ala; C, Cys; D, Asp; E, Glu; F, Phe; G, Gly; H, His; I, Ile; K, Lys; L, Leu; M, Met; N, Asn; P, Pro; Q, Gln; R, Arg; S, Ser; T, Thr; V, Val; W, Trp; and Y, Tyr.
40. Defensin amino acid sequence: HNP-1, HNP-2, and HNP-3, M. E. Selsted, S. S. L. Harwig, T. Ganz, J. W. Schilling, R. I. Lehrer, *J. Clin. Invest.* **76**, 1436 (1985); HNP-4, C. G. Wilde, J. E. Griffith, M. N. Marra, J. L. Snable, R. W. Scott, *J. Biol. Chem.* **264**, 11200 (1989); GPNP, M. E. Selsted and S. S. L. Harwig, *Infect. Immun.* **55**, 2281 (1987); NP-1, NP-2, NP-3a, NP-3b, NP-4, and NP-5, M. E. Selsted, D. M. Brown, R. J. DeLange, S. S. L. Harwig, R. I. Lehrer, *J. Biol. Chem.* **260**, 4579 (1985); and RatNP-1, RatNP-3, and RatNP-4, P. B. Eisenhauer *et al.*, *Infec. Immun.* **57**, 2021 (1989). The RatNP-2 sequence was determined by P. B. Eisenhauer, M. E. Selsted, and colleagues.

41. We thank J. Bowie, G. Fujii, B. Kagan, and A. Pardi for valuable discussions, and NIH for support. Coordinates and diffraction data have been deposited in the Brookhaven Protein Data Bank.

15 October 1990; accepted 20 December 1990

Cross-Regulatory Interactions Between the Proneural *achaete* and *scute* Genes of *Drosophila*

CARMEN MARTÍNEZ AND JUAN MODOLELL

The *achaete* (*ac*) and *scute* (*sc*) genes of *Drosophila* allow cells to become sensory organ mother cells. Although *ac* and *sc* have similar patterns of expression, deletion of either gene removes specific subsets of sensory organs. This specificity was shown to reside in the peculiar regulation of *ac* and *sc* expression. These genes are first activated in complementary spatial domains in response to different cis-regulatory sequences. Each gene product then stimulates expression of the other gene, thus generating similar patterns of expression. Therefore, removal of one gene leads to the absence of both proneural gene products and sensory organs in the sites specified by its cis-regulatory sequences.

THE CUTICLE OF *DROSOPHILA* CARries many sensory organs (SOs). The *achaete* (*ac*) and *scute* (*sc*) genes are necessary for cells to become sensory organ mother cells (SMCs) (*1*). In the imaginal discs that give rise to the adult epidermis, *ac* and *sc* are expressed in groups of cells called the proneural clusters, which delimit the sites where SMCs will develop (*2*). Although these genes are expressed in similar